Chalcogenide Letters Vol. 21, No. 11, November 2024, p. 895 - 915

Harnessing the sunlight to degrade dye using polythiophene-based silver dopped ZnS composite

A. Fatima [a], N. Nadeem [a], Bahaa Saleh [b]. Z. A. Rehan [c], S. Noreen [a], Hafiz T. Ali [b], M. Zahid [a,*]

[a] *Department of Chemistry, University of Agriculture, Faisalabad, Pakistan*
[b] *Department of Mechanical Engineering, College of Engineering, Taif University, Taif 21944, Saudi Arabia*
[c] *Department of Chemistry, School of Science, Sultan Qaboos University Al-Khoud-123, Oman*

The current research work investigated the photocatalytic degradation of dye using polythiophene-based silver-doped zinc sulfide (PT/Ag-ZnS). The ternary composite was synthesized by in-situ chemical oxidation polymerization approach and thoroughly characterized. Maximum photocatalytic activity depicted > 80% for Ag-ZnS and > 94% for PT/Ag-ZnS at pH 7 and 4 respectively at 10 mM oxidant and 30 mg/100 mL catalyst dose, 10 ppm IDC under 90 min. DMSO serves as an effective radical scavenger. The novel polymeric composite exhibits efficient reusability upto five cycles. Pseudo 1st-order kinetic model was best fitted for PT/Ag-ZnS. Toxicity analysis gave a green clue of treated water.

(Received September 1, 2024; Accepted November 11, 2024)

Keywords: Photocatalyst, Conducting polymer, Polymer composites, Ag-ZnS, Hydrothermal, Wastewater treatment

1. Introduction

Freshwater on land is a vital resource for terrestrial life, ecosystems, biodiversity, and human societies [1]. The World Health Organization (WHO) reports that nearly two billion people lack access to clean water for drinking, eating, and sanitation [2]. The scarcity of clean water poses a serious risk to ecosystem sustainability, the natural world, as well as the well-being of people [3, 4]. Recent surveys reveal that at least one month per year, three-quarters of the world's population experience severe water shortages [5]. The increasing water shortfall is primarily attributed to economic growth, population growth, climate change, altered consumption patterns, and an increase in agricultural irrigation [6, 7]. Only 0.1% of the global water supply is usable due to only 2.5% of freshwater reserves being fresh, with most freezing in polar regions and 30% in isolated aquifers [5].

The textile sector produces a million tons of textile byproducts annually, using 50% of dyes lost in effluent [8, 9]. The textile sector annually discharges approximately 200,000 tons of chemical dyes into the ocean [10]. Overuse of dyes on water can prevent light from penetrating, which negatively affects the photosynthesis process of aquatic plants [11]. These dyes are known to be carcinogenic, mutagenic, and teratogenic due to their complex structures and restricted degradation [12]. Developed countries have improved overall quality of life through technology, civic advancements, and available resources [13].

Wastewater removal techniques like physical adsorption, biological degradation, and chemical oxidation face challenges like imperfect degradation, low effectiveness, high costs, and secondary pollution risks [14]. Photocatalysis, an advanced oxidation process (AOP) using semiconductors, is a green, eco-friendly method for converting sunlight into chemical power, promising energy conservation and high efficiency [15, 16]. Antibiotic, bacterium elimination using semiconductor-based photocatalysts has been widely investigated and applied [17-19]. AOPs convert organic contaminants into safe byproducts like water, carbon dioxide, or inorganic ions by

* Corresponding author: rmzahid@uaf.edu.pk
https://doi.org/10.15251/CL.2024.2111.895

using reactive oxygen species (ROS) from oxidants like hydrogen peroxide and persulfates [20, 21]. UV light or solar irradiation forms pairs of electrons and holes in composites, but these charge carriers quickly unite, reducing their effectiveness [22]. AOPs offer a superior method for removing permanent organic pollutants, such as dyes, insecticides, phenolic chemicals, and drugs [23]. By mixing metal sulfides with carbon-based substrates, photo-efficiency is increased, paving the path for innovative visible light-active support-based water treatment systems [24, 25]. Metal sulfides, such as zinc Sulphide, iron Sulphide, cobalt Sulphide, along cadmium Sulphide, have been studied in great detail as photocatalysts due to their smaller bandgaps compared to metal oxides [26]. Noble metal-doped ZnS is crucial for wastewater treatment operations as it enhances photocatalytic efficacy in semiconductor materials [27]. According to the findings, Ag-doped ZnS degrades more quickly than ZnS [28].

Since 2007, CP-based photodegradation has become incredibly popular [29]. Polythiophene (PT), a heterocyclic polymer compound, exhibits a low band gap and excellent stability in both doped and undoped states [30]. PT, despite being challenging to manufacture, is highly demanding due to its exceptional thermal stability and good electrical conductivity [31]. CPs typically exhibit photocatalytic behavior as a result of the prolonged π-conjugation [30]. PT, with a 2.0 eV band gap, exhibits strong photocatalytic properties in UV and visible light and can be efficiently modified by adding functionalities to its main chain [29, 32]. Polythiophene and its nanocomposites offer an intriguing photocatalytic alternative due to their unique electrical properties, environmental sustainability, narrow optical band gap, consistency in doped and neutral forms, and ease of synthesis [29, 33].

According to knowledge, there hasn't been any research on using Polythiophene-based Silver anchored Zinc Sulphide (PT/Ag-ZnS) as photocatalysts for the degrading Rhodamine B (RhB) dye. Therefore, in the current investigation, this research project used hydrothermal and chemical oxidation methods to synthesize Ag-ZnS and PT/Ag-ZnS. Ag-ZnS and PT/Ag-ZnS nanocomposite were tested against Rhodamine B dye for their photocatalytic activity. RhB was chosen as the model dye due to its widespread use in paper-making, textile, printing, and paint industries, and experiments were conducted in the visible range (400–800 nm). These catalysts are characterized using several analysis methods (XRD, FTIR, SEM-EDX). The charge on the surface of the photocatalyst is determined by the Drift method. The long-term stability of the photocatalyst was investigated by Zn leaching test via atomic absorption spectrophotometer (AAS) and an optimization of variables such as pH, oxidant dose, catalyst dose, and time to reaction was carried out. Additionally, the Response Surface Methodology (RSM)'s central composite design was applied to investigate the relationship between each of four distinct variables (catalyst dose, pH, oxidant feed, and along time). Additionally, toxicity, optical analysis, reusability, and scavenging processes were examined too. Furthermore, the kinetic models were also investigated.

2. Experimental section

2.1. Materials

All chemicals and reagents were of analytical grade and used as received without further purification. Anhydrous iron chloride (99%, Uni-Chem), Thiophene (99.5%, Loba Chemie), Chloroform (99.8%, Loba Chemie). Zinc acetate dihydrate [99%, Daejung, Korea). Thiourea (99%, Merck) and silver nitrate (99%, Sigma-Aldrich) were used in this study. Distilled water was used throughout the study.

2.2. Synthesis approach

2.2.1. Synthesis of Zinc Sulfide (ZnS) and Ag-ZnS

Zinc sulfide was obtained by hydrothermal synthesis. The solutions, 0.1 M zinc acetate and 0.1 M Thiourea, were mixed using magnetic stirrer to obtain a clear solution. The mixture was then transferred in Teflon-lined autoclave reactor and placed at 180 °C for for 12 h. Zinc sulfide precipitates were separated using filter paper, washed repeatedly using distilled water/ethanol, and finally dried in an oven at 80 °C. The Ag-ZnS was obtained by repeating the similar method and 0.1

M silver nitrate solution was added during the mixing of zinc acetate and thiourea solutions [34, 35].

2.2.2. Synthesis of polythiophene

To prepare PT chemical oxidation polymerization process was used. A solution of 2 mL of thiophene monomer was poured into a flask containing $CHCl_3$ solution. A solution of 9 g of $FeCl_3$ was then added to 180 ml of $CHCl_3$. It was mixed thoroughly before adding this mixture to thiophene in a $CHCl_3$ stirring solution. After that, the mixture was constantly stirred for about 24 hours. The precipitate was stirred for 24 hours before being filtered out. At 100 °C, the solution had been dried out for 90 minutes. A pestle and mortar were used to turn the finished product into a powder [36].

$$C_4H_4S + FeCl_3 + CHCl_3 \rightarrow -(C_4H_4S) - + FeCl_2 + CHCl_3 \quad (1)$$

2.2.3. Synthesis of PT/Ag-ZnS

The chemical oxidation polymerization technique was utilized to prepare the PT/Ag-ZnS composite. Ag-ZnS solution that had been hydrothermally synthesized was treated ultrasonically for about 20 minutes and then put into a flask that held 2 mL of thiophene monomer solution (soln 2). Subsequently, 180 mL of $CHCl_3$ was added to 9 g of $FeCl_3$, being thoroughly mixed to prepare a uniform mixture of (soln.3). After that, for 24 hours, both solns. 2 and 3 were continually stirred magnetically in a 1:1 ratio. After stirring for 24 hours, the precipitates that resulted had been filtered out. At 100 °C, the mixture had been dried out for about 90 minutes. A pestle and mortar were used to turn the finished product into fine powder.

2.3. Characterization

Utilizing various methods, the prepared catalysts (Ag-ZnS and PT/Ag-ZnS) were characterized. With the aid of a scanning electron microscope with energy-dispersive X-ray equipment (SEM-EDX JEOL/EO JSM-5910), the morphological along with elemental examination of catalysts was carried out. Using Agilent Technologies' Fourier Transform Infrared Spectroscope, or FT-IR the existence of several functional groups was identified [37]. The size of the crystallite was determined utilizing the Debye-Scherrer equation, while the phase characterization of the produced materials was captured by an X-ray diffractometer (XRD, Rigaku) fitted with a Cu-K radiation source (=0.154056 nm) at an operational current as well as 45 kV and 40 mA of voltage, correspondingly. The energy gaps in the band of photocatalysts were estimated utilizing the CECIL CE 7200 UV-visible spectrophotometer, and the % degradation of samples that were treated was examined [41]. Employing AAS (Z-8200, Japan; Hitachi Polarized Zeeman AAS), a Zn leaching analysis of a Rh B treated dye solution was carried out under the parameters recommended in the AOAC [37].

2.4. Photocatalytic degradation

The photocatalytic decomposition tests were conducted in the presence of visible light from the sun. However, visible irradiations were used to optimize for factors including pH, oxidant dose, catalyst dose, and my period. The LUX meter or a solar power meter (SM206) was utilized to measure the light brightness of sunshine (2 ×2 ft). In the current study, rhodamine B (RhB) was chosen as a model dye. To conduct the degradation investigation, 100 mL of a 10 ppm (RhB) solution was used. Each adjusted parameter was combined with a blank or control experiment and exposed to sunlight. The RhB solution did not degrade noticeably in a control without a catalyst or oxidant added, proving that photolysis was not significant for the RhB solution in the control experiment. 0.1 M NaOH with 0.1 M HCl solutions were used to change the pH of the solution.

To achieve the greatest likelihood of interactions among the catalyst and subsequently dye molecules, it was subjected to a 1 min ultrasonic treatment. H_2O_2 (at a specific concentration) was then added to the reaction mixture following sonication. From 12 p.m. to 2 p.m., the entire setup was put in direct sunshine, and dye solutions were continuously shaken in an orbital shaking device (Pamico Technologies) at a speed of shaking that was roughly 150 rpm. Before being subjected to sunlight, the solutions were stirred for about 30 min in the dark to reach an equilibrium between adsorption and desorption. The dye mixtures were tested after evaluating the photocatalysts' capacity for adsorption. For the separation of the composites, 3mL of the solution of dye that had been treated

had to be centrifuged following each run. To evaluate the amount of the dye following treatment with sunlight irradiation, the treated solution's absorption of dye was determined by a UV-VIS spectrophotometer (CECIL CE 7200) at 550 nm (RhB max = 550 nm) wavelength. An empty beaker holding a solution of dye was kept in the dark as well as in the sunlight to examine how quickly the dye degraded in both the darkness and the presence of light. We calculated the % degradation using the following equation (Eq). Following a comparison of treated and untreated dye solutions' absorption rates, the percentage degradation was calculated.

$$Degradation\ (\%) = (1-\frac{C_t}{C_o}) \times 100 \quad (2)$$

However, C_f=final concentration and C_o=initial concentration. To test the reusability of the catalysts, they were recycled five times, every time in ideal conditions with sunshine and a freshly made 10 ppm RhB solution. This was found to assess the cost-effectiveness of PT/Ag-ZnS by determining its maximum use. For optimization, these two catalysts (Ag-ZnS and PT/Ag-ZnS) were used.

2.5. Kinetics

For a comprehensive understanding of the reaction process, kinetic studies are crucial. Various kinetic models are typically used to describe the kinetics of dye degradation. In the present research work, the whole process of RhB degradation was studied by using two kinetic models, namely the 1st-order kinetic model Eq. (5) and the 2nd-order kinetic model Eq. (6). For each catalyst, the reaction pathway of the degradation of dye was modeled using the most appropriate approach.

$$\boldsymbol{ln\frac{C_o}{C_t} = K_1 t} \quad (3)$$

$$\boldsymbol{\frac{1}{C_t} - \frac{1}{C_o} = K_2 t} \quad (4)$$

2.6. Response surface methodology (RSM)

A statistical approach called RSM, which stands for Response Surface Methodology, can be used to improve a process such as photocatalytic oxidative decomposition of organic contaminants. It combines mathematical and statistical methods to provide a more reliable manner of interaction between experimental parameters that can be controlled. By using statistical designs for experiments, this methodology aids in the simultaneous modeling of two or more variables. RSM can be used to forecast the successful assessment of the model as well as cumulative response.

The central composite design (CCD)-under RSM was employed in this study. The benefit of CCD is that the design provides adequate information with comparatively fewer runs of experiments. Providing total cost-efficiency using experiments in this way. The subsequent formula was used to execute 20 trials using 8 factorial, 6 axial, as well as 6 central duplicates to establish the goodness of fit for the 23 multifactorial CCD using three different variables (dye dose, oxidant dose, along with catalyst dose);

$$\mathbf{N = 2^n} + 2n + n_c = 2^3 + 2 \times 3 + 6 = 20$$

whereas,

N = total no of runs

n = the number of factors used in runs

pH (A), catalyst dose (B), as well as oxidant dose (C), represented the independent variables, and the response factor was the percentage % of RhB degradation.

Every independent variable had a total of five levels: Xi = 1.68, 1.68, 1.68, and 1.68. For interpreting the relationship between each of the three independent variables (oxidant dose, dye dose, along catalyst dose), the least square test with a second-order model was chosen, and the response variable was % degradations. The second-order model's expression is given below Eq. (6);

$$Y = \beta \circ + \sum_{i=1}^{K} \beta_i X_i + \sum_{i=1}^{K} \beta_{ii} X_i^2 + + \sum_{i=1}^{K} \cdot \sum_{i \neq j=1}^{K} \beta_{ij X_i X_j} + \varepsilon \quad (5)$$

Here, Y represents the response factor (i.e., the % degradation), is the numeric coefficient, which is i for linear effects, ii for interacting effects, and ii for quadratic effects. Independent k variables make up the number "ij," and "epsilon" (ε) denotes random error. Three replicate trials are conducted at the center point for the error-free estimation in CCD. Random studies have been carried out to reduce the response's confusing variability. utilizing "Design Expert 13.0" software, response surfaces including contour plots for RhB dye degradation utilizing PT/Ag-ZnS (1:1) in the specified range of conditions were generated. By statistically computing F-values at a probability parameter (p) of 0.05 (F-test) as well as goodness of fit (R^2), the suitability and reliability of models were assessed according to their statistical significance.

3. Results and discussion

3.1. Structural and morphological characterizations

The range of 400–4000 cm $^{-1}$ has been examined in the FTIR spectrum analysis. The findings are displayed in Figure 1a. Shakir et al (2024) reported that different IR active vibration modes have been reported, each exhibiting distinct peaks. The measured ZnS peaks are located at 935 and 679 cm^{-1}. The C=O stretching modes were suggested by the peaks ranging from 1550–1750 cm^{-1}. The The peaks at 711 cm $^{-1}$, 787 cm $^{-1}$, 1192 cm $^{-1}$, 1316 cm $^{-1}$ and 1623 cm −1 indicated the synthesis of PT. FTIR spectra indicated the successful synthesis of photocatalysts [35, 38].

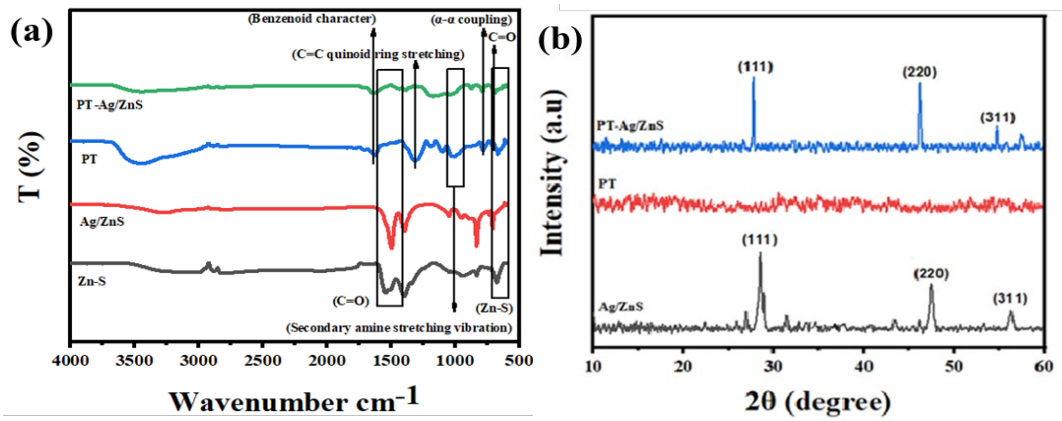

Fig. 1 (a) FTIR spectrum of ZnS, Ag-ZnS, PT, and PT/Ag-ZnS and (b) XRD spectrum of Ag-ZnS, PT, PT/Ag-ZnS. [35].

Shakir et al (2024) reported that X-ray diffraction has been used to determine the crystal structure and crystalline phase of the prepared materials, as illustrated in Figure 1b. XRD analysis of Ag-doped ZnS showed diffraction peaks at 28.9°, 47.8°, and 56.5° at 2Θ. These were identified as the crystallographic planes of (111), (220) as well as (311), indicating (JCPDS: 01-080-0020) [35, 39-41]. The presence of low-intensity wide peaks for the PT indicates that the produced polythiophene has an amorphous nature. The Ag-ZnS crystals exhibit a significant peak shifting in their planes (111), (220), and (311), from locations of peaks 28.9°–27.6°, 47.8°–46.0°, and 56.5°–54.8°. This is a result of impurity ions being successfully introduced into the PT backbone [35].

The surface geometries and microscopic details of materials were analyzed in detail using several scanning electron microscopy (SEM) resolutions in Figure 2. Figure 2a illustrates the irregular geometrical sphere form of Ag-ZnS, which features deeper surface bends. It is anticipated that this will improve the specific surface area and make targeted molecule enrichment easier. The amorphous composition of PT is indicated by the irregular and macro-granular nonporous structure

of the polythiophene in Figure 2b. e [42]. The in-situ integration of Ag-ZnS, as shown in Figure 2c, has been demonstrated by the growth Ag-ZnS nanostructures on the PT surface. The composite, which was made of Ag-ZnS nanoparticles and fibers of polythiophene, has a structure similar to a tangled web and resembles granules having sharp lateral edges [43].

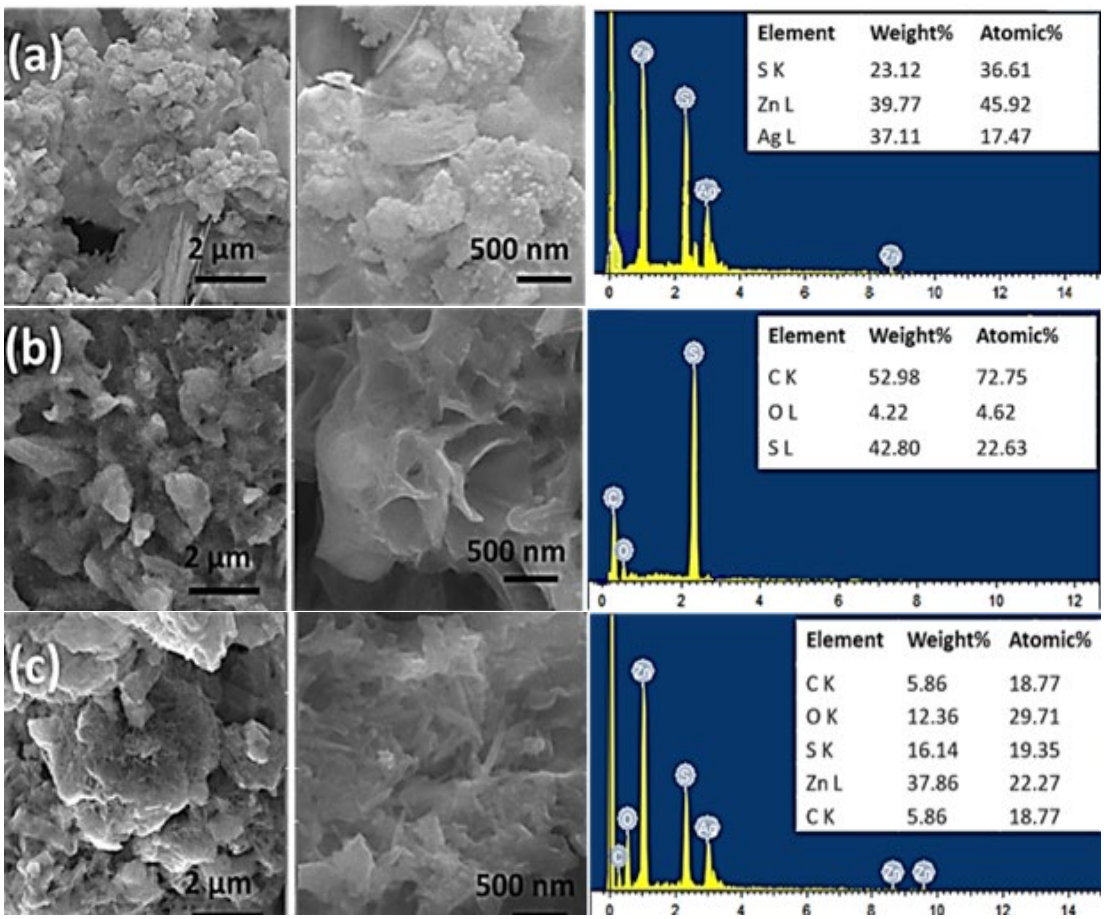

Fig. 2. SEM-EDS representation of (a) Ag-ZnS, (b) PT, (c) PT/Ag-ZnS nanocomposite.

EDS investigation analysis was used to examine the surface chemical analysis, and elemental composition, in addition to the positions of many essential elements, as shown in *Figure 2 (right side)*. The weight % of each element found in nanocomposites is displayed in an inserted table. Ag-ZnS composite's analysis using EDS reveals an appearance of peaks for zinc (Zn), sulfur (S), and silver (Ag). Zinc (Zn), sulfur (S), silver (Ag), carbon (C), and oxygen (O) are present in PT/Ag-ZnS. Along with other key elements, sulfur is found in PT/Ag-ZnS at 16.14 weight percent (wt%), showing the hybrid production of Ag-ZnS with polythiophene.

3.2. Point of zero charges

The pH "drift technique" was utilized to determine the synthetic composite's point of zero charges (Pzc) as described in Figure *3*. To get rid of any dissolved carbon dioxide (CO_2) a 0.01 M solution of sodium chloride was made and heated. The initial pH level of the NaCl solution was adjusted by diluting both HCl and NaOH solutions. To get rid of any dissolved CO_2, a set of five bottles of glass with caps that contained 50 mL of the sodium chloride (NaCl) solution were sterilized with N_2 gas. Drops of both NaOH or HCl solutions were added as needed to the solutions in glass bottles to bring the pH_i values to a range of (3–11). Every bottle received 0.10 g of catalyst before being sealed and stirred for 24 hrs. in an orbital shaker. The pH of the equilibrium mixture

was checked. The intercept at the x-axis of the displayed pH value pH_f against pH_i represented the Pzc readings for the catalyst.

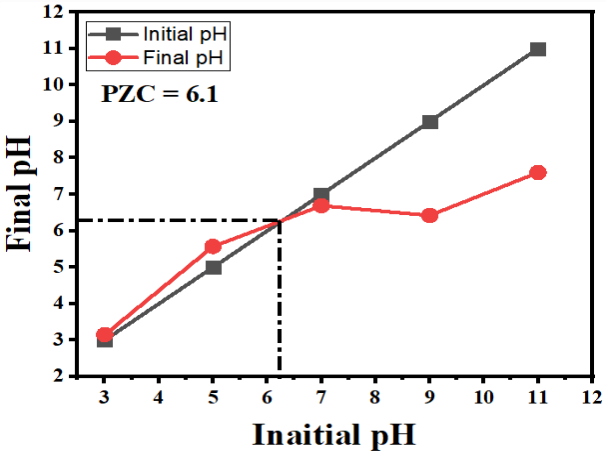

Fig. 3. Point of Zero charge of PT/Ag-ZnS.

3.3. Optical analysis

It was feasible to determine the bandgaps of Ag-ZnS as well as PT/Ag-ZnS using UV-visible spectra. Using the suggested formula in Eq. (8), estimations of the catalysts' bandgap energy were derived.

$$(ahv)^2 = (hv - Eg) \tag{6}$$

The Ag-ZnS's bandgap is approximately 3.03 eV. Because of the composite creation with polythiophene, the bandgap of PT/Ag-ZnS was lowered from 3.03 eV to 2.6 eV. The bandgap shrunk, increasing the efficiency of PT/Ag-ZnS as photocatalytic activity. The high bandgap makes it necessary for electrons to be excited more significantly as they transition between the conduction band (CB) and the valence band (VB) [44].

The main reason for the poor photocatalytic efficiency of Ag-ZnS is the broad energy band [45]. When comparing the bandgaps of Ag-ZnS with PT/Ag-ZnS, the graph showed that Ag-ZnS addition in PT reduced the band gap to (2.6 eV), which increased the photocatalytic properties of PT/Ag-ZnS as described in Figure 4. By adjusting the edge flaws and surface modifications of implanted polythiophene sheets, The PT/Ag-ZnS efficacy can be easily enhanced by Charge carrier transport challenges. Altering the energy levels of associated materials as well as the emergence of novel energy levels resulting from the functionalization of groups, ultimately affects the electrical characteristics of those materials [46]. In addition, the Ag-ZnS nanocomposites composed of polythiophene are said to have extraordinary photodegradation effectiveness in the sun's visible spectrum. The existence of PT reduces the bandgap as well as improves the sensitivity to sunlight [47]. As separation charge carriers for a longer duration of time, this ultimately suppresses the rate of charge-carrier recombination, improving the photostability and efficiency of catalysts [48].

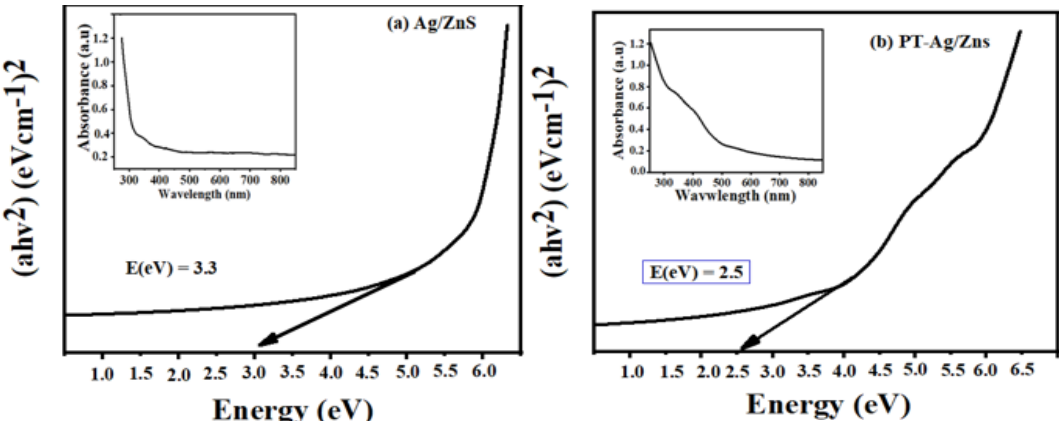

Fig. 4. Estimating bandgap energies using the Tauc plot method and displaying each nanocomposite's UV–VIS absorption spectrum.

3.4. Optimization of parameters affecting the rate of dye degradation

3.4.1. Effect of pH

The most significant operational variable for influencing the photocatalytic decomposition of contaminants over Ag-ZnS and PT/Ag-ZnS composites is pH. The photocatalyst surface and the ionization process of the dye are both influenced by the solution's pH. In the range of pH values of 2 to 9, the impact of pH was investigated. Other variables were held constant while evaluating the impact of pH on RhB breakdown. According to research, RhB degradation was shown to be more pronounced at pH 7 for Ag-ZnS and pH 4 for PT-Ag/Zn composite materials.

Dye was degraded by Ag-ZnS in acidic conditions (83%), basic conditions (76%), and pH 7, where it degraded by a percentage of 85% as showin in Figure 5a. For PT/Ag-ZnS, the % degradation was 89% under acidic environments, 73% under basic circumstances, and 94% at pH 4 conditions. A greater amount of adsorption effectively influenced RhB's photocatalysis during the dye degradation mechanism. The surface of the photocatalyst and the pH of the solution have a significant impact on adsorption. For example, a basic or acidic pH causes the photocatalyst surface to protonate or deprotonate Protonated sites that are active on a substance called photocatalyst surface are responsible for the lower pH. Additionally, RhB is a cationic dye. *Figure 5b* depicts the breakdown of RhB; the findings show that the surface of the catalyst is negatively charged at a higher pH level and positively charged at a lower pH [49].

For instance, the mixture is highly charged with H+ ions at a pH of only 3, which would combine with hydroxyl radicals to form H_2O thus lowering the value for the amount of OH Eq. (9)

$$HO^{\cdot} + H^{+} + e^{-} \rightarrow H_2O \tag{7}$$

However, the Fenton-like process of reaction in the solution is responsible for the catalysts' reported degradation around acidic pH levels [50]. By interacting with hydroxyl ions, this causes the creation of additional hydroxyl radicles. Increased photocatalytic RhB degradation is achieved as a result of suppressing the recombination of species that are charged [51]. It was discovered that the photocatalytic breakdown of RhB was negatively impacted by pH values exceeding 7 for Ag-ZnS and pH levels more than 4 for PT/Ag-ZnS. The OH radicals combine to create hydrogen peroxide at greater values of pH that are not optimal, therefore RhB cannot be oxidatively degraded at those pH levels depicted in Eq. (10) [50].

$$HO^{\cdot} + HO^{\cdot} \rightarrow H_2O_2 \tag{8}$$

The electrostatic attraction between molecules of substrate and the "active" areas of composites can be used to explain how pH affects photooxidation effectiveness. The interaction was predicted to increase the likelihood that the resultant hydroxyl radicle would come into contact with

molecules of Dye [52]. According to conventional wisdom, the overall degradation reaction will either be accelerated or suppressed depending on the dominant factors, and they might be attractive or repelling. The type of contact was governed by the intrinsic characteristics of the polymer. The amine (NH_2) group functions as both an electron donor as well as an exchange of cations in a chemical interaction. Additionally, conducting polymers are capable of nonpolar associations [49].

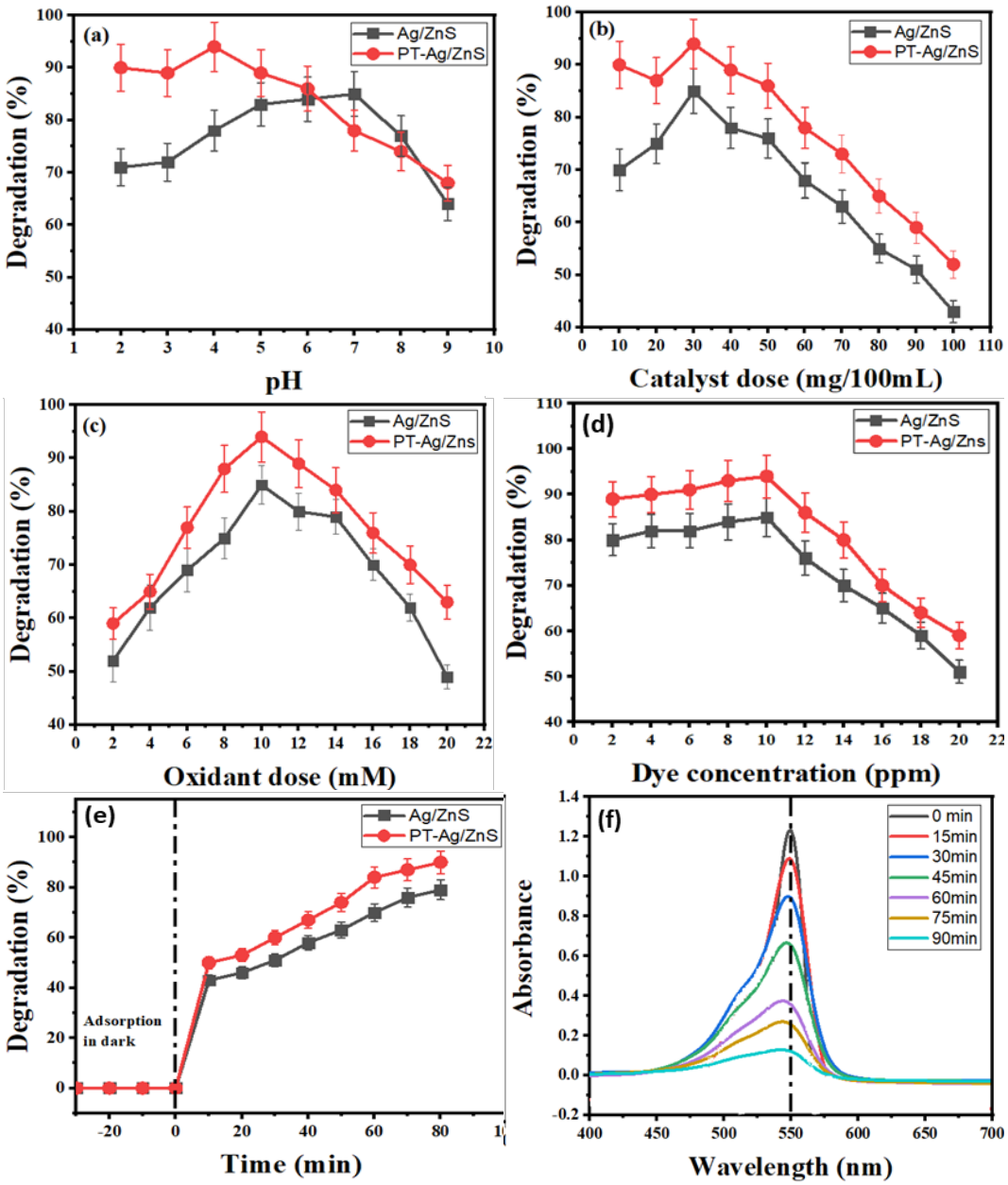

Fig. 5. Optimization of various operating parameters (a) pH, (b) catalyst dose, (c) H_2O_2 dose, (d) dye concentration, (e) reaction time, and (f) Spectral Scans concerning degradation time.

3.4.2. Effect of photocatalyst concentration

The amount of surface area of catalysts has a significant impact on their catalytic effectiveness. The proper amount of catalyst must be chosen as a result to maximize degrading efficiency. For Ag-ZnS and PT/Ag-ZnS, the influence of different catalyst doses (10–100 mg/100 mL) on degradation effectiveness has been studied under the optimal conditions of pH (4,7), oxidant dose (10 mM), as well as reaction time (90 min). Decreased efficiency of degradation was seen for

the level of catalyst employed in the process of degradation, as shown in *Figure 5b*. However, as the catalyst dosage was increased, the rate of degradation accelerated (i.e., at 30 mg/100 mL for Ag-ZnS and 30 mg/100 mL for PT/Ag-ZnS: Figure 5b because there were more effective and sufficient active sites available. On the other hand, with an additional rise in the c feed of catalyst over 3 mg/100 mL for Ag-ZnS and PT/Ag-ZnS, a drop in degrading efficiency was observed. The aggregation of the catalyst, which caused stacking of nanoparticles over each other, resulting in them being less available to be used for adsorption, resulting in the photocatalytic decomposition of dye, was suggested as the potential cause of the drop in degradation efficacy. Additionally, the high catalyst concentration may result in the dispersion of UV radiation. Therefore, it was hypothesized that decreased sunlight penetration was to blame for the decline in UV-assisted $HO^{\cdot}$ radical production, which in turn led to decreased dye degradation [53, 54].

3.4.3. Effect of oxidant dose

When examining how different organic contaminants respond to photocatalytic decomposition, an oxidant plays a significant role. Dye degradation is facilitated by a suitable catalyst-to-oxidant ratio. Therefore, to achieve the highest dye degradation while maintaining the other factors constant, a wide range of the concentrations of hydrogen peroxide (H_2O_2; 1-20 mM) as an oxidizing agent was used in *Figure 5c*.

Catalysts are made more effective for the degradation of organic dyes by a radical called hydroxyl ($HO^{\cdot}$). As H_2O_2 is required for capturing electrons for the production of radicals with hydroxyl groups, RhB degradation often happens after its addition [55]. This $HO^{\cdot}$radical production accelerates the breakdown of the dye RhB as it binds to the catalyst surface. When accepting electrons from the CB that produces $HO^{\cdot}$, a crucial active species for the degradation process, new active sites are simultaneously created [56].

$$H_2O_2 + O_2^{-} \rightarrow HO^{-} + HO^{\cdot} + O_2 \tag{9}$$

$$H_2O_2 + e^{-}(CB) \rightarrow HO^{\cdot} + HO^{\cdot} \tag{10}$$

According to the results, maximal degradation was attained at H_2O_2 concentrations of 3 mM for Ag-ZnS and 10 mM for PT/Ag-ZnS. Degradation efficiency was found to decrease both below and above the optimal value. It was hypothesized that the low oxidant concentrations (1-8 mM for Ag-ZnS and PT/Ag-ZnS) did not produce enough OH radicals to fully degrade RhB. By raising the oxidant quantity, greater degradation was seen, reaching its maximum value (>80%) for Ag-ZnS at 10 mM and its maximum value (94%) for PT/Ag-ZnS at 10 mM too. However, as H_2O_2 concentration increased, the effectiveness of photocatalytic breakdown decreased. The coupling of OH and $HO^{\cdot}$radicals caused a decrease in degrading efficiency, which oxidizing species deactivation. Moreover, the higher amount of $OH^{\cdot}$ either competes with the adsorption of dye molecules [57].

$$H_2O_2 + HO^{\cdot} \rightarrow H_2O + HOO^{\cdot} \tag{11}$$

$$HOO^{\cdot} + HO^{\cdot} \rightarrow H_2O + O_2 \tag{12}$$

3.4.4. Effect of dye concentration

The amount of dye that has been adsorbed upon the surface of the catalyst has a significant impact on how much dye is degraded. All other parameters, meanwhile, were maintained at their ideal values. One of the primary influencing variables for dye degradation is the impact of various starting dye concentrations on its photocatalytic breakdown. As can be seen in *Figure 5d*, the rate for degradation increased gradually with a high starting RhB concentration before stabilizing. The initial dye concentration ranged between 2 and 20 ppm/100 mL, Ag-ZnS and PT/Ag-ZnS showed the best degradation at 10 ppm/100 mL, with 85% and 94%, respectively. Further rises in concentration had an inhibiting effect on the degradation process. The following result could be explained by the fact that the active site saturation brought on by the adsorption of molecules of the substrate is reducing the production of activated radicles.

Another potential for minimal degradation at elevated B concentrations is the creation of several chemical intermediates, some of which remain around the catalyst's surface for a considerable amount of time. Minimal interaction among reactive species and new RhB molecules occurs as a result. Increased dye molecule concentrations and the resulting intermediates capture more photons throughout the reaction period and reduce the number of photons available for catalyst stimulation. Surface-initiated freely reactive radicles that would otherwise degrade RhB are prevented from forming by a complete saturation of the surface by molecules of a reactant or produced as intermediates through adsorption/sheer agglomeration in the immediate region. Because of this, the ideal concentration in the current circumstance is only helpful when certain experimental conditions are satisfied [58].

3.4.5. Effect of irradiation time

The most important aspect in influencing the photocatalyst's degradation activity was the irradiation time. The original dye quantity, catalyst dose, oxidant dosage, along pH had been kept constant throughout time optimization. The Ag-ZnS as well as PT/Ag-ZnS photocatalysts were used in the present study. The Ag-ZnS photocatalyst displayed 85% after 90 minutes, while PT/Ag-ZnS displayed 94%, respectively *Figure 5e*. The RhB degradation scans concerning time are presented in *Figure 5f*. The increased charge carrier production generated by visible irradiations has been credited for enhanced catalytic degradation. A common photocatalytic process produces an e^-/h^+ pair at a certain source of radiation (sunlight) with energy equivalent to or higher than the photocatalyst's bandgap energy. Furthermore, it lessens the electron-hole pair's tendency to recombine. For sunlight, the LUX meter recorded light levels between 98,000 ± 2000 lx.

3.4.6. Reusability/stability

The analysis of the stability of the photocatalyst materials has been completed up to four subsequent cycles of reusability under optimal conditions and is shown in Figure *6a*. After the process of reaction was completed under ideal circumstances, the used photocatalyst was recovered via centrifugation, cleaned, and dried in an oven before being reused. It was measured how much was left over. The photocatalytic composite was isolated and employed under the same circumstances after each cycle. After five times of reuse, the catalyst recovery yield slightly falls (by about 11%), whereas the percentage degradation for Ag-ZnS and PT/Ag-ZnS decreases from 85% to 54% and 94% to 77 correspondingly. The blocking or deactivation of more than one active site may be the reason for the decreased degradation of photocatalytic efficiency, changing the physical and chemical characteristics of the catalysts. The aggregation of byproducts on the surface of the photocatalyst that restricts the active sites was unexpectedly linked to the decreased efficiency of the catalyst after repeated treatment. After each run, a steadily declining activity of the photocatalyst was observed.

After being reprocessed five times, the composite still had photocatalytic activity. This demonstrates the photocatalyst's strong stability along with reusability. Minimal leaching during the reaction medium's phase transition from solid phase to liquid phase is a requirement for the stability of metal-based catalysts in the treatment of wastewater. As a result, Atomic Absorption Spectroscopy (AAS) was used to evaluate the leaching of Zn for the PT/Ag-ZnS catalyst after five cycles. AAS analysis results in little Zn leaching (0.5 mg/L), ensuring good catalyst stability. Directives from the European Union state that the Zn value should not be higher than 5.0 mg/L. The Zn leaching value in the current investigation is significantly lower than the EU Directives. After five reusability cycles, materials modestly reduced photocatalytic degradation efficiency may be attributable to the blocking and/or reduction in the total number of functioning sites caused by repeated use.

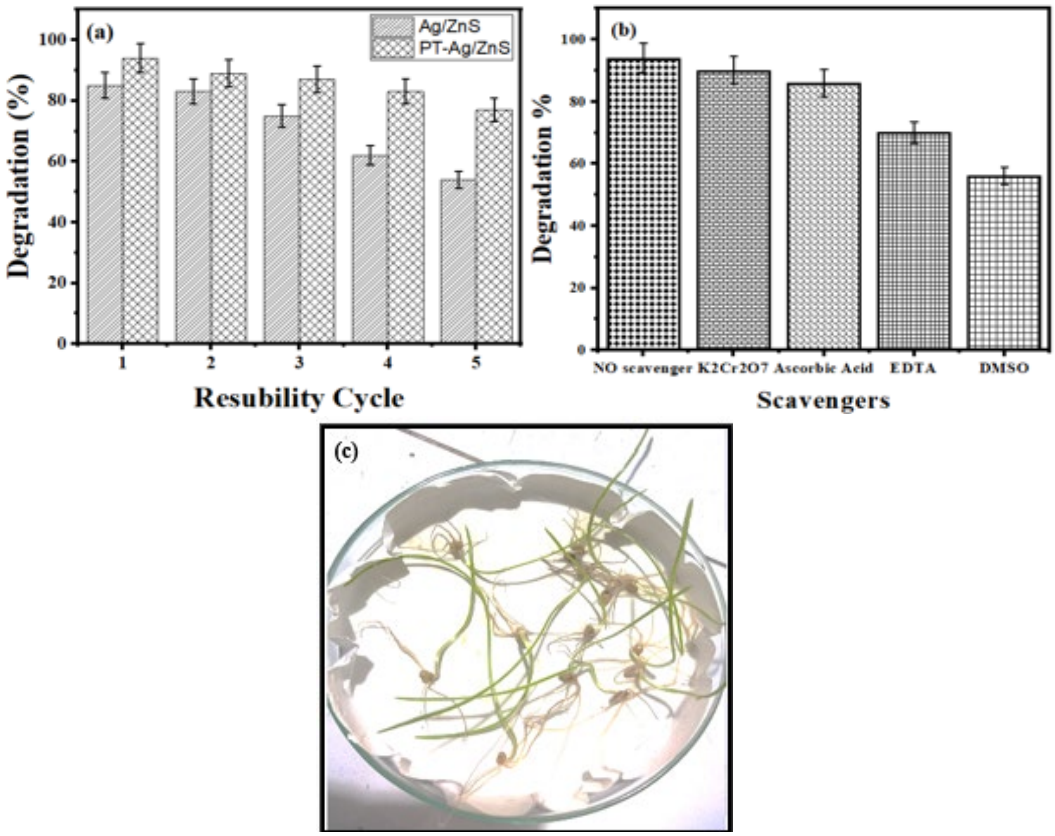

Fig. 6. Reusability Cycle (a) Scavengers activity (b) and Toxicity analysis (c).

3.4.7. Radical scavenging experiment

The existence of active species radicles which are significant in photocatalysis was examined using various scavengers. With the incorporation of catalyst to RhB, tests for radical scavenging have been conducted under ideal conditions for pH, catalyst dosage, dye concentration, oxidant quantity, and time duration. Different scavengers, including potassium dichromate ($K_2Cr_2O_7$) for electron (e), dimethyl sulfoxide (DMSO) for hydroxyl radicals ($HO^{\cdot}$), ascorbic acid (AA) for superoxide radicals ($O^{2\bullet}$), using a hole (h^+) scavenger called disodium ethylene diamine tetraacetate (EDTA-2Na), have been included to the reaction the mixture for this prospect 5 mM of scavenger was added to a dye mixture as part of the experiment. The solution was then held when there was light that could be seen, and a variation in the concentration of RhB was seen at a wavelength of 550 nm. According to Figure *6b*, the sequence of reduced photocatalytic efficiency following the addition of scavengers to the reaction medium is DMSO> EDTA>AA>$K_2Cr_2O_7$>no scavenger. The fact that DMSO significantly hindered RhB's photocatalysis suggests that the hydroxyl ion ($HO^{\cdot}$) for PT/Ag-ZnS was the primary source of the degradation process. After DMSO, EDTA significantly reduced degradation, showing that holes (h+) played a significant role in a chemical system. A smaller degree than in the situation of $K_2Cr_2O_7$, the decomposition of dye is also prevented by the incorporation of ascorbic acid (AA) to provide superoxide radical ($O_2^{\bullet}$). Using the results of this test, a potential RhB's mechanism for increased photocatalysis PT/Ag-ZnS is displayed in Figure 7[59].

Results showed that PT is primarily responsible for the composite's improved performance. It offers increased adsorption capacity, electrical conductivity, as well as active sites for the process of adsorption. In a catalyst, the valance band (VB) towards the conduction band (CB) transition of the electrons was activated. The photoexcited electrons were quickly collected and transported to the surface by polythiophene's strong electronic conductivity, which effectively prevented the resulting recombination of charges and caused the holes and electrons to generate extremely hydroxyl ions that are reactive. For degradation, PT/Ag-ZnS nanocomposite is an excellent and

efficient photocatalyst material of dye as a result of the synergistic effects of adsorption as well as photocatalysis.

3.4.8. Wastewater treatment for reuse and toxicity analysis

Gardening, irrigation of outdoor areas, and irrigation of crops are only a few uses for the wastewater that has undergone either primary as well as secondary treatment. The organic contaminants are converted to CO_2 during the oxidation procedures used for treating wastewater, and water can then be used for restoring surface freshwater. Because of environmental and societal factors, it is becoming common to grow edible crops utilizing wastewater that has been treated using sunlight-active composites [60]. It is critical to establish the effectiveness of the dye-contaminated treatment of wastewater method using conductive polymer nanocomposite under sunlight. This is dependent on the type of by-products that are created. The most fragile wheat crop seeds were treated with RhB-treated water using PT/Ag-ZnS for this purpose. Seeds with filter papers and glass caps were soaked in the 10 mL processed RhB dye water. For 24 hours, the Petri plates had been kept at ambient temperature. As can be shown in Figure *6c*, the wheat seeds exhibited significant germination. Additionally, utilizing the RhB-treated wastewater did not cause the seeds to become black, indicating the water is safe to be utilized for the irrigation of crops [61, 62].

3.5. Proposed charge transfer mechanism via PT/Ag-ZnS

An outline diagram showing the decomposition of RhB dye caused by photogenerated charge carrier/transformation is depicted in Figure 7. The radicals called hydroxyl along with holes that are thought to play important functions in the dye the degradation process is the basis for the proposed mechanism. Based on the information we comprehend, the electrons and holes responsible for the photodegradation mechanism are created when greater amounts of light are absorbed than bandgap electrons, along with holes are generated that cause the degradation procedure to start and are created immediately as the surface of the composite is irradiated with energy.

The lowest as well as highest unoccupied molecular orbitals (LUMO and HUMO, respectively) in PT are positioned at E_{VB} = -3.12 and E_{CB} = -5.20 eV [63]. Compared to ZnS, the energy levels associated with PT tend to be more negative. When exposed to light, the HOMO of PT's electrons moved to the LUMO, rendering holes left behind. The conduction band (CB) of ZnS absorbed these photogenerated electrons. By absorbing electrons that escape from the CB of ZnS, doping of ZnS with Ag enhances the prevention of electron/hole pair recombination in ZnS. The conversion of oxygen to superoxide radicles is aided by these electrons. In the meantime, water along with the holes in ZnS's valence band (VB) combine to form hydroxyl radicles [64]. The following factors may be responsible for the increased photocatalytic efficiency of the PT/Ag-ZnS composite. First of all, Ag doping enhances ZnS's charge separation.

The second step is the efficient transmission of electrons from PT's LUMO to ZnS and then to Ag is the result of the energy bands of PT and ZnS working well together. Thirdly, the PT's conjugated structure allows it to speed up the transfer of holes [65]. On the fourth no when Ag-ZnS and PT are combined, the active sites (particularly surface area) expand, resulting in better pollutant adsorption and photocatalysis. Additionally, when dye molecules are excited by light, an electron is transferred to a photocatalyst, which then reacts with a schematic oxygen molecule that forms $O.^{-2}$ along with other active radicals during the oxidation process [66]. Last, but not least, the lower band gap of PT, which is 2 eV, encourages the electrons to move to the larger band gap of Ag-ZnS, which is 3.03 eV, in the proper order, degrading dye molecules by radical generation method via oxidation as well as reduction process [38].

$$\mathrm{PT-Ag-ZnS} + \mathrm{hv} \rightarrow \mathrm{PT}(\mathrm{e^-(CB)} + \mathrm{h^+(VB)}) + Ag/ZnS\left(\mathrm{e^-(CB)} + \mathrm{h^+(VB)}\right) \quad (13)$$

$$\mathrm{PT}(\mathrm{e^-(CB)} + \mathrm{h^+(VB)}) + Ag/ZnS\left(\mathrm{e^-(CB)} + \mathrm{h^+(VB)}\right) \rightarrow \mathrm{PT}(\mathrm{h^+(VB)}) + Ag/ZnS\left(\mathrm{e^-(CB)}\right) \quad (14)$$

$$\mathrm{e^-} + \mathrm{O_2} \rightarrow \mathrm{O_2^-} \quad (15)$$

$$\mathrm{h^+} + \mathrm{HO^-} \rightarrow \mathrm{HO\cdot} \quad (16)$$

$$HO^{\cdot} + \text{RhB dye} \rightarrow CO_2 + H_2O \quad (17)$$

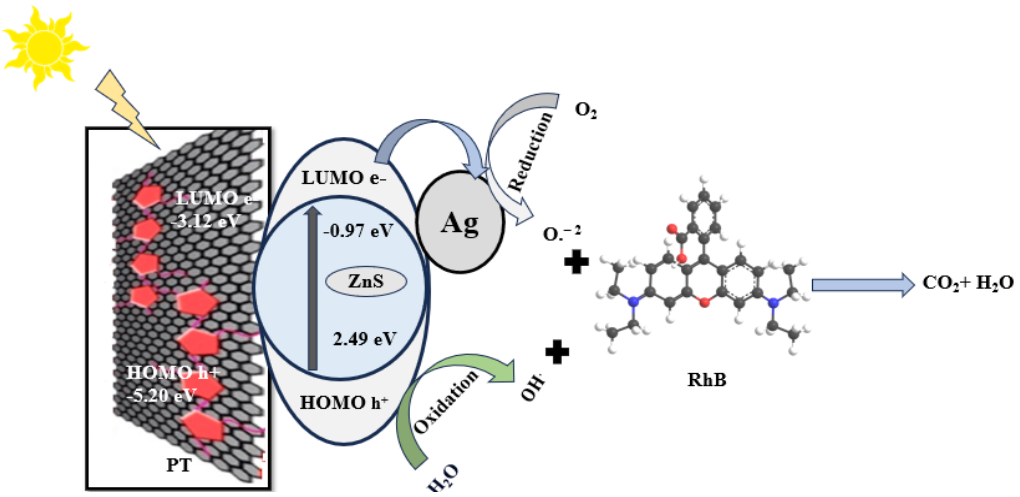

Fig. 7. Schematic diagram of the proposed mechanism of PT/Ag-ZnS composite on RhB Dye.

3.6. Kinetics of photodegradation reaction

Using the experimental data, first- and second-order kinetic models were used to investigate the RhB degradation kinetics [67, 68]. A straight-line relationship between "t" and "ln Co/Ct" is seen in Figure *8*. Table 1illustrates that the first-order kinetics model is superior to the second-order model for simulating the process of photocatalytic degradation since it exhibits a greater value for Adj R^2.

Here, The initial dye solution concentration at time zero was denoted by "Co," while the precise time represented by "t" was indicated by "Ct." [69]."K_1" as well as"K_2" are the rate constants of 1st order and 2nd order reactions. The plot of time vs ln (Ct/Co) showed a straight-line result. The value of k was examined utilizing a 1st-order slope. In PT/Ag-ZnS the anchoring of Silver into ZnS and combining it with PT increased degradation activity as indicated by a high Adjusted R-square value.

Table 1. Kinetic parameters of 1st order kinetics and 2nd order kinetics.

	1st-order reaction kinetics	**2nd order reaction kinetics**
Adj. R-square	0.98	0.84
Intercept	-0.78102 ± 0.06303	-3.28338 ± 1.34821
Slope	0.01244 ± 0.00134	0.15886 ± 0.02396

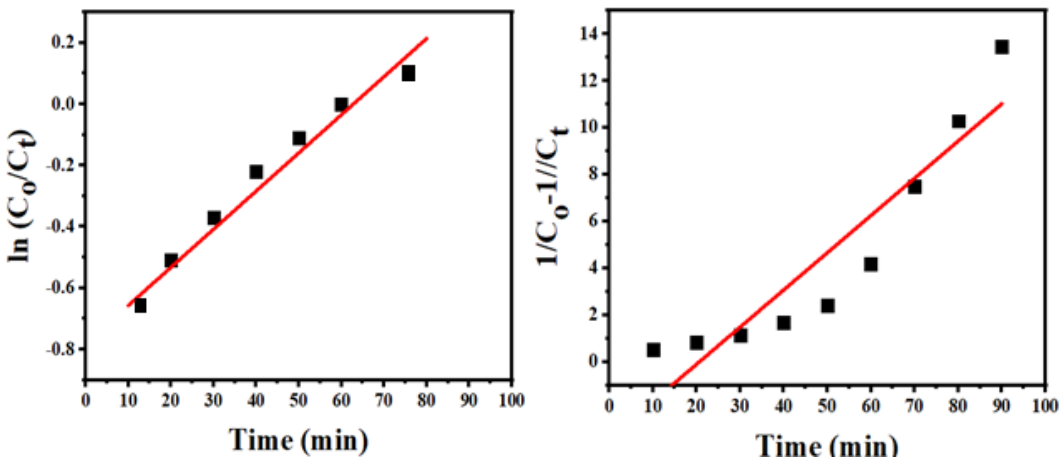

Fig. 8. Reaction kinetics (a) pseudo-1st order, (b) 2nd-order kinetic model of Ag-ZnS, PT/Ag-ZnS.

3.7. Response surface methodology

The Response Surface Methodology (RSM) is groundbreaking in the optimization of several elements involved in the photocatalytic decomposition process. The Central Composite Design (CCD) methodology was employed as part of this research to look at how different factors affected how quickly Rhodamine B decayed. The management of independent elements, such as pH, oxidant dosage, and catalyst quantity, was made possible through the usage of Central Composite Design (CCD), which allowed for the greatest amount of decomposition (the value associated with the response variable).

3.7.1. Analysis of variance (ANOVA)

The model's fit summary plot clearly shows how much the used model affects the variables that have been optimized. The highly significant predictive potential of the model is also demonstrated by its higher R^2 value (Table 2). It was found that there exists a strong correlation between variables including pH, oxidant dosage, catalyst quantity, and the degree of degradation whenever a quadratic formula was applied. The relationship between the components mentioned above and the percentage of RhB dye that deteriorated was examined using the second-order polynomial relationship Eq. 25. Here, Y stands for the dependent variable's response (% degradation), β ◦is a coefficient with a specific value, i is a linear coefficient, and ii is a quadratic coefficient. In contrast, it is used to denote the coefficient value for interaction effects. Additionally, xi and xj indicate coded readings for independent factors, while ε stands for random error.

$$Y = \beta \circ + \sum_{i=1}^{K} \boldsymbol{\beta}_i \boldsymbol{X}_i + \sum_{i=1}^{K} \boldsymbol{\beta}_{ii} \boldsymbol{X}_i^2 + + \sum_{i=1}^{K} \cdot \sum_{i \neq j=1}^{K} \boldsymbol{\beta}_{ij X_i X_j} + \varepsilon \quad (25)$$

Lack of ft along with regression analysis determines the model ft for specific information. The P-value informs us whether a variable is significant or not. The model is no longer significant if p>0.1000, however, it is still significant if p <0.0001.

$$Y = 94.01 + 2.31 * A + -0.8820 * B - 0.0732 * C - 1.63 * AB + 1.62 * AC + 0.1250 * BC + - 4.11 * A2 + - 1.29 * B2 + - 4.64 * C2 \quad (26)$$

The quantities of the oxidant, pH, and catalyst, respectively. A2, B2, and C2 show quadratic effects, while AB, AC, and BC show a straight-line relationship among independent variables. *Figure 9a* depicts the effects of altering the pH and catalyst concentration. The association between the variables is shown on a three-dimensional display as well as a contour map. The study was carried out using a catalyst dosage of 10-100 mg/100 mL and a pH value range of 2-9. The degradation rate increases from 2 to 9 pH levels, reaching a high at 4 pH before declining. At pH 4, Fenton-like processes are what cause the most dye degradation.

Table 2. Analysis of variance (ANOVA)Table for RhB degradation using PT/Ag-ZnS.

Source	**Sum of squares**	**Df**	**Mean square**	**F-value**	**P-value**	
Model	634.24	9	70.47	57.24	< 0.0001	significant
A-pH	72.65	1	72.65	59.02	< 0.0001	
B-catalyst dose	10.62	1	10.62	8.63	0.0148	
C-Time	0.0732	1	0.0732	0.0595	0.8123	
AB	21.13	1	21.13	17.16	0.0020	
AC	21.12	1	21.12	17.16	0.0020	
BC	0.1250	1	0.1250	0.1015	0.7565	
A^2	243.85	1	243.85	198.08	< 0.0001	
B^2	23.80	1	23.80	19.33	0.0013	
C^2	310.78	1	310.78	252.45	< 0.0001	
Residual	12.31	10	1.23			
Lack of fit	12.31	5	2.46			
Pure error	0.0000	5	0.0000			
Cor. Total	646.55	19				
Std. dev.	1.11		R^2	0.9810		
Mean	87.15		Adjusted R^2	0.9638		
C.V. %	1.27		Predicted R^2	0.8478		
			Model precision	19.7738		

Between 10 and 30 mg/100 mL of concentration of catalyst was also improved in the photocatalytic decomposition of RhB. Maximum Decomposition was reached after 30 mg and no significant changes have been noticed. The reason for this enhancement is that the greater photocatalyst surface area provides more dye adsorption sites. Nanoparticle coagulation and subsequent blockage of active sites happen with higher catalyst concentrations. As a result, when exposed to sunshine, a photocatalyst destroys an object more slowly.

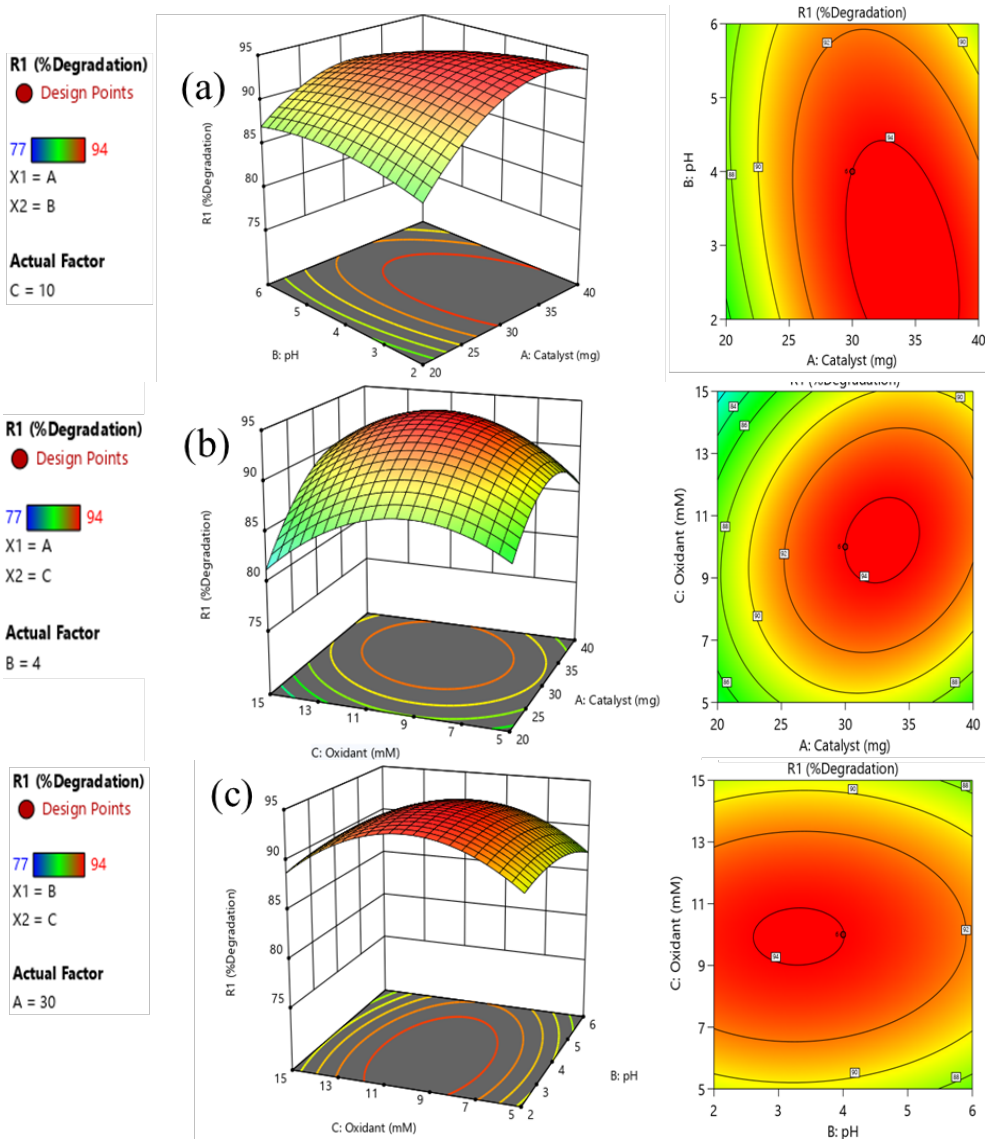

Fig. 9. 3D and contour plots of (a) pH and catalysts conc., (b)Oxidant and Catalyst dose, (c)Oxidant dose and pH.

In Figure 9b, the catalyst and oxidant dose are depicted. The optimum oxidant dose ranged from 1 mM to 20 mM, with 10 mM showing the highest degradation. Increasing the catalyst concentration did not further accelerate degradation. The combination of OH·− OH·, which caused the oxidizing entity to become inactive, was linked to the drop in degrading efficiency. Additionally, the dye molecules may have competition for adsorption due to the excessive amount of OH·.

Five confirmation experiments were carried out by RSM under the ideal environment to verify the conclusions drawn using the CCD statistical analysis. The computer generated a total of five alternatives for ideal conditions by suitability requirements. The viability of experimental statistical approaches for experimental data was then validated by choosing one methodology for additional experiments. Oxidant concentration of 10 mM/100 mL, catalyst dose of 30 mg /100mL, and pH 4 were the ideal conditions for degradation. The average rate of degradation proved to be 94%. The experimental decomposition of dye values was thought to be extremely near to the RSM-predicted value. These results demonstrate the predictability of the dye degradation model in an experimental environment [70].

4. Conclusion

Wastewater treatment ensures that access to clean water is recycled for the sustainable growth of the ecosystem on Earth. This research project revealed the potential of PT/Ag-ZnS nanocomposite to clean the RhB-contaminated water up to 94% greater than binary composite. The % degradation effectiveness resulted in the incorporation of polythiophene in Ag-ZnS composite that enhanced the physiochemical properties to elevated promising levels. The electrical conductivity of PT leads to the mobility of charges due to π- conjugation resulting in a desired candidate for photocatalysis as PT/Ag-ZnS catalyst due to enhanced reaction kinetics because of functionalities like doping of silver in Zns and its integrated structural composition. Response surface methodology (RSM) shows best fit up to 98% of the model. Kinetics fits the model to a 1st-order significant model. Concluding remarks predicted the enhanced % degradation of up to 94 % of dye in wastewater with Zn-leaching 0.5mg/L in water as safe water for irrigation purposes.

Consent for publication

All the authors agree to publish this article.

Conflict of interest

The authors declare no competing interest

Acknowledgments

The authors extend their appreciation to Taif University, Saudi Arabia, for supporting this work through project number (TU-DSPP-2024-91).

Funding

This research was funded by Taif University, Saudi Arabia, Project No. (TU-DSPP-2024-91).

References

[1] Kumar, R., et al., Biodiversity and Bioeconomy. 2024, Elsevier. p. 347-380; https://doi.org/10.1016/B978-0-323-95482-2.00016-X

[2] Zuarez-Chamba, M., et al., Environmental Research, 2022. 209: p. 112834; https://doi.org/10.1016/j.envres.2022.112834

[3] Gleick, P.H., H. Cooley, Annual Review of Environment and Resources, 2021. 46: p. 319-348; https://doi.org/10.1146/annurev-environ-012220-101319
[4] Zhao, D., et al., Resources, Conservation and Recycling, 2021. 175: p. 105834; https://doi.org/10.1016/j.resconrec.2021.105834
[5] Shehata, N., et al., Chemosphere, 2023. 320: p. 137993; https://doi.org/10.1016/j.chemosphere.2023.137993
[6] Qin, Y., et al., Nature Sustainability, 2019. 2(6): p. 515-523; https://doi.org/10.1038/s41893-019-0294-2
[7] Richter, B.D., et al., Nature Sustainability, 2020. 3(4): p. 319-328; https://doi.org/10.1038/s41893-020-0483-z
[8] Madkhali, N., et al., Results in Engineering, 2023: p. 100920; https://doi.org/10.1016/j.rineng.2023.100920
[9] Acharya, R., A. Lenka, K. Parida, Journal of Molecular Liquids, 2021. 337: p. 116487; https://doi.org/10.1016/j.molliq.2021.116487
[10] Abdullah, F., N.A. Bakar, M.A. Bakar, Journal of hazardous materials, 2022. 424: p. 127416; https://doi.org/10.1016/j.jhazmat.2021.127416
[11] Donkadokula, N.Y., et al., Reviews in environmental science and bio/technology, 2020. 19: p. 543-560; https://doi.org/10.1007/s11157-020-09543-z
[12] Badvi, K., V. Javanbakht, Journal of Cleaner Production, 2021. 280: p. 124518; https://doi.org/10.1016/j.jclepro.2020.124518
[13] Lechevallier, M. M. Buckley, Clean Water: What is acceptable microbial risk. Series Clean water: What is acceptable microbial risk, 2023.
[14] Zhao, D.L., et al., Water Research, 2024: p. 121111; https://doi.org/10.1016/j.watres.2024.121111
[15] You, J., et al., Carbohydrate Polymers, 2022. 288: p. 119332; https://doi.org/10.1016/j.carbpol.2022.119332
[16] Zhang, M., et al., Journal of Colloid and Interface Science, 2022. 615: p. 663-673; https://doi.org/10.1016/j.jcis.2022.02.026
[17] Mustafa, F.S., A.A. Oladipo, Journal of Water Process Engineering, 2021. 42: p. 102132; https://doi.org/10.1016/j.jwpe.2021.102132
[18] Oladipo, A.A., A.O. Ifebajo, M. Gazi, Applied Catalysis B: Environmental, 2019. 243: p. 243-252; https://doi.org/10.1016/j.apcatb.2018.10.050
[19] Mustafa, F.S., A.A. Oladipo, Chemosphere, 2023. 312: p. 137348; https://doi.org/10.1016/j.chemosphere.2022.137348
[20] Wang, J., S. Wang, Journal of Cleaner Production, 2021. 315: p. 128202; https://doi.org/10.1016/j.jclepro.2021.128202
[21] Liu, G., et al., Environmental Research, 2023: p. 116534; https://doi.org/10.1016/j.envres.2023.116534
[22] Rahman, K.H., A.K. Kar, Journal of Environmental Chemical Engineering, 2020. 8(5): p. 104181; https://doi.org/10.1016/j.jece.2020.104181
[23] Akter, S., et al., Arabian Journal of Chemistry, 2022. 15(7): p. 103900; https://doi.org/10.1016/j.arabjc.2022.103900
[24] da Silva, S.W., et al., Current Pollution Reports, 2021. 7: p. 146-159; https://doi.org/10.1007/s40726-021-00176-6
[25] Camargo-Perea, A.L., et al., Ultrasonics Sonochemistry, 2021. 73: p. 105500; https://doi.org/10.1016/j.ultsonch.2021.105500

[26] Koulini, G., et al., Chemosphere, 2022. 289: p. 133152; https://doi.org/10.1016/j.chemosphere.2021.133152
[27] Choi, Y.I., et al., Journal of Alloys and Compounds, 2016. 675: p. 46-56; https://doi.org/10.1016/j.jallcom.2016.03.070
[28] Yazdani, E.B., A. Mehrizad, Journal of Molecular Liquids, 2018. 255: p. 102-112; https://doi.org/10.1016/j.molliq.2018.01.154
[29] Zia, J., F. Fatima, U. Riaz, Catalysis Science & Technology, 2021. 11(20): p. 6630-6648; https://doi.org/10.1039/D1CY01129D
[30] Bundgaard, E., F.C. Krebs, Solar Energy Materials and Solar Cells, 2007. 91(11): p. 954-985; https://doi.org/10.1016/j.solmat.2007.01.015
[31] Chen, X., et al., Chemical reviews, 2010. 110(11): p. 6503-6570; https://doi.org/10.1021/cr1001645
[32] Garg, S., N. Goel, Journal of Molecular Graphics and Modelling, 2022. 117: p. 108285; https://doi.org/10.1016/j.jmgm.2022.108285
[33] Majumder, A. A.K. Gupta, Journal of Environmental Chemical Engineering, 2020. 8(6): p. 104463; https://doi.org/10.1016/j.jece.2020.104463
[34] Zahid, M., H.F. Shakir, Z.A. Rehan, Journal of Thermoplastic Composite Materials, 2023. 36(4): p. 1489-1503; https://doi.org/10.1177/08927057211064990
[35] Shakir, H.M.F., et al., Synthetic Metals, 2024: p. 117687; https://doi.org/10.1016/j.synthmet.2024.117687
[36] Shanmugapriya, C., G. Velraj, Optik, 2016. 127(20): p. 8940-8950; https://doi.org/10.1016/j.ijleo.2016.06.075
[37] Farhan, A., et al., Scientific Reports, 2023. 13(1): p. 9497; https://doi.org/10.1038/s41598-023-36486-6
[38] Mazhar, S., et al., Environmental Science and Pollution Research, 2022: p. 1-15.
[39] Allahveran, S., A. Mehrizad, Journal of Molecular Liquids, 2017. 225: p. 339-346; https://doi.org/10.1016/j.molliq.2016.11.051
[40] Harish Kumar, A., et al., Journal of Inorganic and Organometallic Polymers and Materials, 2021. 31: p. 2003-2016; https://doi.org/10.1007/s10904-020-01869-z
[41] Agarwal, S., et al., Journal of Molecular Liquids, 2016. 218: p. 494-498; https://doi.org/10.1016/j.molliq.2016.02.040
[42] Thanasamy, D., D. Jesuraj, V. Avadhanam, Polymer, 2019. 175: p. 32-40; https://doi.org/10.1016/j.polymer.2019.03.042
[43] Tahir, N., et al., Journal of Environmental Management, 2023. 337: p. 117706; https://doi.org/10.1016/j.jenvman.2023.117706
[44] Shinde, S.G., et al., Journal of Environmental Chemical Engineering, 2020. 8(3): p. 103769; https://doi.org/10.1016/j.jece.2020.103769
[45] Kumar, A., et al., Materials Today Communications, 2024. 38: p. 108252; https://doi.org/10.1016/j.mtcomm.2024.108252
[46] Lv, R., et al., Rare Metals, 2022. 41(2): p. 639-649; https://doi.org/10.1007/s12598-021-01759-4
[47] Tahir, S., et al., Environmental Science and Pollution Research, 2023: p. 1-19; https://doi.org/10.1007/s11356-023-31096-1
[48] Preetha, R., et al., Journal of Alloys and Compounds, 2022. 904: p. 164038; https://doi.org/10.1016/j.jallcom.2022.164038
[49] Khan, F., et al., International Journal of Environmental Science and Technology, 2023. 20(5): p. 4811-4826; https://doi.org/10.1007/s13762-022-04283-9

[50] Nadeem, N., et al., International journal of Environmental Science and Technology, 2021: p. 1-16; https://doi.org/10.1007/s13762-021-03255-9
[51] Satdeve, N., R. Ugwekar, B. Bhanvase, Journal of Molecular Liquids, 2019. 291: p. 111313; https://doi.org/10.1016/j.molliq.2019.111313
[52] Tahir, S., et al., Viral and Antiviral Nanomaterials. 2022, CRC Press. p. 139-164; https://doi.org/10.1201/9781003136644-9
[53] Meena, P.L., et al., Biomass Conversion and Biorefinery, 2022: p. 1-17; https://doi.org/10.1007/s13399-022-02605-y
[54] Rahman, M.U., et al., Optical Materials, 2021. 120: p. 111408; https://doi.org/10.1016/j.optmat.2021.111408
[55] Tahir, S., et al., Fuel, 2021. 305: p. 121502; https://doi.org/10.1016/j.fuel.2021.121502
[56] Chu, W., W. Choy, T. So, Journal of hazardous materials, 2007. 141(1): p. 86-91; https://doi.org/10.1016/j.jhazmat.2006.06.093
[57] Visa, M., C. Bogatu, A. Duta, Journal of Hazardous Materials, 2015. 289: p. 244-256; https://doi.org/10.1016/j.jhazmat.2015.01.053
[58] Mustapha, F., et al., Journal of Cleaner Production, 2017. 168: p. 1150-1162; https://doi.org/10.1016/j.jclepro.2017.09.095
[59] Asgari, E., et al., Process Safety and Environmental Protection, 2019. 128: p. 65-76; https://doi.org/10.1016/j.psep.2019.05.050
[60] Singh, A., Resources, Conservation and Recycling, 2021. 168: p. 105454; https://doi.org/10.1016/j.resconrec.2021.105454
[61] Khan, M., et al., Optik, 2023. 290: p. 171282; https://doi.org/10.1016/j.ijleo.2023.171282
[62] Mfarrej, M.F.B., et al., Journal of Plant Growth Regulation, 2023. 42(3): p. 1402-1420; https://doi.org/10.1007/s00344-022-10674-6
[63] Yan, W., et al., Rsc Advances, 2014. 4(62): p. 33039-33046; https://doi.org/10.1039/C4RA05578K
[64] Ali, H., E.S. Mansor, Colloid and Interface Science Communications, 2020. 39: p. 100330; https://doi.org/10.1016/j.colcom.2020.100330
[65] Zhang, R., et al., Separation and Purification Technology, 2020. 234: p. 116098; https://doi.org/10.1016/j.seppur.2019.116098
[66] Alam, U., et al., Catalysis Today, 2017. 284: p. 169-178; https://doi.org/10.1016/j.cattod.2016.11.037
[67] Tabasum, A., et al., Plants, 2020. 10(1): p. 6; https://doi.org/10.3390/plants10010006
[68] Kaur, J., A. Gupta, O. Pandey, Solar Energy, 2018. 176: p. 678-687; https://doi.org/10.1016/j.solener.2018.10.077
[69] Fan, T., et al., Materials Science in Semiconductor Processing, 2015. 40: p. 439-445; https://doi.org/10.1016/j.mssp.2015.06.054
[70] Lau, W., A. Ismail, Membr Water Treat, 2010. 1(1): p. 49-60; https://doi.org/10.12989/mwt.2010.1.1.049